Characterizing the Great Lakes hydrokinetic renewable energy resource

Farhadzadeh, Ali; Hashemi, M. Reza ; Neill, Simon

Energy

DOI:
10.1016/j.energy.2017.04.064

Published: 01/06/2017

Peer reviewed version

Characterizing the Great Lakes Hydrokinetic Renewable Energy Resource: Lake Erie Wave, Surge and Seiche Characteristics

Farhadzadeh, Ali, Stony Brook University, Stony Brook, NY 11779
Hashemi, M. Reza, University of Rhode Island, Narragansett, RI 02882
Neill, Simon, Bangor University, UK

ABSTRACT

Lake Erie is the fourth largest, in surface area, of the Great Lakes. Seiching events in the lake have in the past led to breaches of the flood wall in Buffalo (at the eastern end of the lake), causing loss of life, and significant loss to properties. Here, we analyze the potential of Lake Erie for generating electricity from its storm surge, seiching, and wave energy resources. We find that there is significant potential energy in the lake that may be suitable for generating meaningful levels of electricity from seiches and storm surge; for instance, by developing an artificial 'lagoon'. It is shown that an extreme surge event similar to that of January 30, 2008 which generated a surge of approximately +3 m at the eastern end and a corresponding set-down of nearly -2.7 m at the western end of Lake Erie, could contain a total theoretical potential energy of approximately 5×10^7 kWh. If such energy could, practically, be harnessed using a surge lagoon with a surface area of 2 km^2 near Buffalo, the potential energy would be 2.3×10^4 kWh, enough energy to power the equivalent of 40 homes for an entire month. The cost of such a lagoon could be partially offset by the potential of such a structure, and the operation of such a lagoon, to help alleviate flooding during extreme events. Furthermore, as an example, the analysis of the lake-wide wave data for 2011 shows that the monthly mean wave power is greater in the central and eastern basins of Lake Erie. Wave power was highest in October and November when the monthly mean wave power reached 10 kW/m. In contrast to most oceanographic environments, the wave power resource is reduced in winter, mostly due to the presence of surface ice in the lake. The surface ice appears to significantly reduce wave height and power during winter months, resulting in a relatively low annual mean wave power. However, the monthly mean wave power was the lowest in late spring and during summer when the monthly mean wave power was around 2.5 kW/m. Although this study represents the first attempt to assess the marine renewable energy of Lake Erie, further research is necessary to examine the feasibility of energy extraction in the lake.

1. INTRODUCTION

As the world population continues to grow against a backdrop of increasing economic development and urbanization, the demand for energy continues to grow. There are, however, limited fossil fuel reserves to meet the world's energy demands, and so more sustainable and less polluting renewable sources of electricity generation are sought, including hydrokinetic energy.

The Electric Power Research Institute (EPRI) estimated the annual energy potential from wave energy along the outer shelf (notional 200 m depth contour) and inner shelf (notional 50 m depth contour) of the US East Coast as 237 TWh and 172 TWh, respectively. In the state of New York, the annual available wave energy resource along its outer and inner shelf was estimated to be 16 TWh and 12 TWh, respectively [1]. However, the report does not account for the renewable wave energy potential of the Great Lakes bordering this state, *i.e.* Lake Ontario and Lake Erie. A study by the New York State Energy Research and Development Authority (NYSERDA) suggested that, if fully developed, the available primary renewable resource without regard for cost, social, or technological restrictions, could supply 41% of New York State's total primary energy demand by 2030. If energy for transportation is excluded from the projection, renewable resources have the technical capacity to supply 54% of the State's total energy needs by 2030. Based on an assessment, in 2010, less than 10% of New York State's total energy demand, including transportation, was supplied by renewable energy [2]. This estimate does not include the resources available in the Great Lakes, which contain about 21% of the world's surface fresh water. Among the Great Lakes, Lake Erie with a surface area of approximately 26,000 km^2, is the fourth largest

and the smallest in volume [3]. It is also the eleventh largest lake in the world, bordering with States of New York, Pennsylvania, Ohio, and Michigan in the US, and the Province of Ontario in Canada.

Offshore wind energy of the lake has attracted some interest among communities and researchers. Lake Erie Energy Development Corporation (LEEDCo) was initiated in 2009, as a nonprofit organization, to develop offshore wind energy in Lake Erie. A 20.7 MW wind project off the Ohio coast has been planned as a pilot project to demonstrate the feasibility of offshore wind, and to facilitate and expedite future offshore wind projects [4]. The suitability of offshore wind projects in this area has been reported in the academic literature (*e.g.*, [5]).

Lake Erie's hydrokinetic renewable energy resources are characterized through this study. Firstly, Lake Erie's characteristics and the data used in this study are presented. Then, the method and tools used for the analyses of the data are described, namely in situ and numerical modelling. Following this, the results are presented, and finally some conclusions are made.

2. METHODS

Historical water level data collected at several National Oceanic and Atmospheric Agency's (NOAA), as well as Canada's Department of Fisheries and Oceans, water level stations were analyzed to identify short-term extreme events (*i.e.*, storms). Return period analysis of the extreme events was carried out to determine the frequency of occurrence of the events. The primary goal here is to propose a potential methodology to harness extreme surge and seiche energy by adapting the tidal lagoon concept (*e.g.*, [6]) which could also alleviate coastal flooding in coastal Lake Erie. The extreme event analysis will also provide information regarding the magnitude and number of extreme events per year that could be used to estimate annual energy of storm surge and seiching in the lake that could be extracted using the lagoons.

To characterize the levels of energy associated with various modes of seiching, spectral analysis of long-term hourly lake level time-series were carried out, and the power spectral density (PSD) of the water levels at various locations around the lake developed.

A two-dimensional coupled circulation and spectral wave model was used to simulate lake-wide variation of the lake level during storms. The potential energy contained in individual extreme events was estimated using the predicted water level during extreme events.
Lake Erie undergoes extensive surface ice cover during winter months. The effect of ice cover on storm surge was quantified by comparing the lake level responses to atmospheric forcing under the actual ice-covered, and a hypothetical ice-free lake for a storm event.

To characterize wave energy in Lake Erie, historical wave data from three active wave buoys were used. Furthermore, lake-wide monthly averaged wave power maps were developed and presented for year 2011, selected as an example. The maps are generated based on the hindcast wave data provided by the US Army Corps of Engineers (USACE).

2.1. Study Area

Lake Erie's length and width are approximately 400 km and 90 km, respectively. Lake Erie has mean and maximum depths of about 20 m and 63 m, respectively (see Figure 1).

The water levels in Lake Erie undergo various cycles of changes at intra- and inter-annual timescales. Short-term lake level variation occurs due to storm surge induced by high wind and low pressure systems moving over the Great Lakes region. The historical water level data shows that eastern Lake Erie experiences storm surges of up to 3 m. Annual lake level change occurs due to seasonal climate variability that affects the amount of water flowing into and out of Lake Erie, the contribution of groundwater, and precipitation & evaporation directly into and from the lake. The lake level is normally highest during late spring and early summer, and lowest during winter. Long term fluctuations are primarily due to deviation from the average climatic condition. For instance, higher or lower than average precipitation occurring in several successive years can deviate the long term water level from its average.

Climate change is expected to result in more powerful, more frequent, and longer duration storms in the Great Lakes basin [7]. Lake Erie, the shallowest of the Great Lakes, is known for its high storm surge and low frequency oscillations (*i.e.*, seiches). Following a strong wind blowing along the longer axis of the lake from Toledo in the southwest toward Buffalo in the northeast (the predominant wind direction), or vice versa, standing waves or seiches are developed in the lake, travelling back and forth and rotating counterclockwise around the lake until their energy dissipates. A combination of factors, including water level, waves, and currents, results in extreme events that can cause flooding and erosion in coastal areas. A seiche event in 1844, considered as "one of the greatest natural disasters in Buffalo's recorded history", reportedly "occurred without warning, breaching the 4.5 m floodwall, flooding the waterfront, and drowning at least 78 people" [8]. In 2008, a powerful storm that created up to 5 m high waves and a storm surge of about 3 m resulted in flooding near Buffalo [9]. Analysis of water level and flow rate data shows that the impact of seiche waves can potentially extend beyond the lake, especially along streams and rivers.

Lake Erie's seiche has been the subject of several early studies [10]. Attempts were made to identify the frequencies corresponding to the modes of free oscillations based on limited lake level data. Spectral analyses showed that low frequency oscillations of the lake level were more energetic during winter than summer, but less concentrated at the frequencies related to the first and second seiching modes. Using standard harmonic analysis, the tidal amplitude and phase of lunar semidiurnal tides was determined. The tide is insignificant in Lake Erie. A counterclockwise rotation of high water level corresponding to diurnal and lower order seiches was identified using spectral analysis of limited lake level data [11,12,13]. The relationship between meteorological forcing and water level oscillation in Lake Erie was studied using wind and water level data [14,15,16]. The propagation of seiche waves under ice-free and ice-covered Lake Erie was studied and it was found that the surface ice can suppress the low frequency oscillations of the lake water level [17].

As the shallowest of the five Great Lakes, Lake Erie warms up more rapidly in summer, and freezes over in winter more frequently and more extensively than the other lakes. Almost every winter, Lake Erie is characterized by extensive surface ice. The historical ice data show that the Annual Maximum Ice Cover (AMIC) index, defined as the maximum percentage lake surface area covered by ice during a given year, was greater than or equal to 80% between 1973 and 2014, with the exception of 6 winters. The ice data also reveal that in the recent years, Lake Erie experienced less severe winters, resulting in lower levels of surface ice concentrations [18].

2.1.1. Lake Erie Location and Bathymetry

Lake Erie is one of the five Great Lakes. On the US side, it borders the states of New York, Pennsylvania, Ohio and Michigan. There are a number of major cities along the Lake Erie shoreline which include Buffalo in New York; Erie in Pennsylvania; Toledo, Sandusky and Cleveland in Ohio. On the Canadian side, Port Stanley in Ontario borders Lake Erie.

Figure 1 shows the location of Lake Erie among the Great Lakes, as well as the bathymetric information of Lake Erie. As noted earlier, the lake is the shallowest among the Great Lakes. Its western basin is about 60 km long, and is very shallow. It extends to 11 m depth. The eastern basin, the deepest of the three basins, has a maximum depth of 63 m and is about 130 km long. The central basin is wider and longer than the other basins. It extends to 25 m depth, and has a length of about 210 km [19].

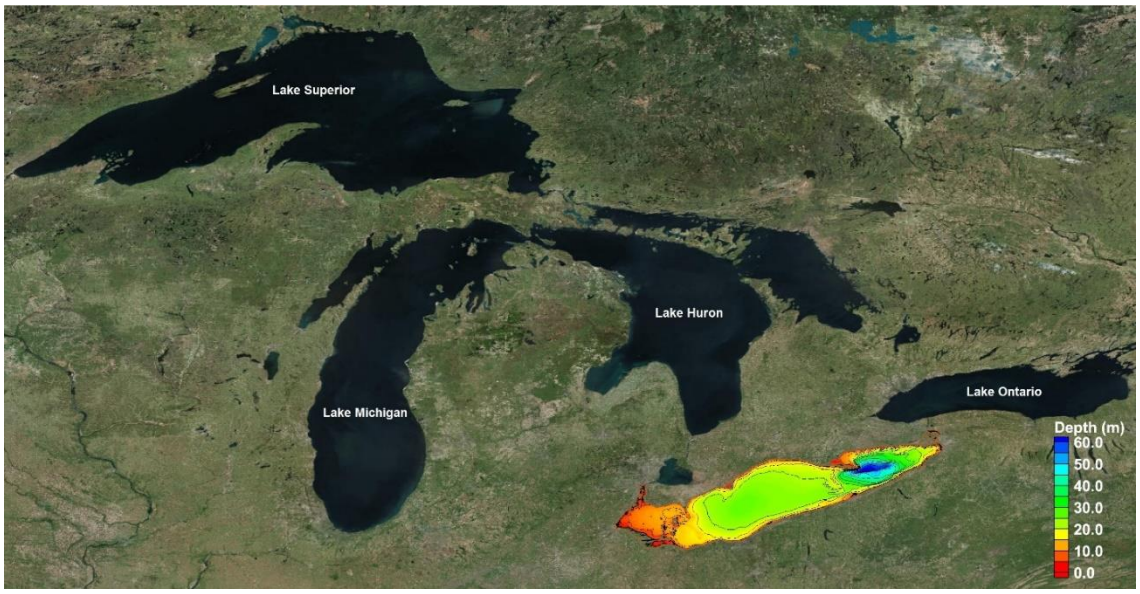

Figure 1. Lake Erie bathymetry and location among Great Lakes

2.2. Data

In the following sub-sections, the data used in this study are described in detail. These data include water level and wave data.

2.2.1. Ice Data

The Great Lakes ice season typically begins in January and ends in April. The ice data are collected through aerial imagery on a daily, weekly or bi-weekly basis, and archived in the Ice Atlas database. The spatial resolution of the ice data for the period of 1973 – 2002 is 2.8 km by 2.8 km, and its temporal resolution is weekly or bi-weekly. The digital ice data after 2002 has better grid resolutions, ranging from 1.25 km to 2.5 km. The temporal resolution varies from daily, for the most recent years, to half-weekly for older data sets [20].

2.2.2. Wave Data

Lake Erie's wave data include data recorded by the wave buoys and the hindcast data generated through the US Army Corps of Engineers' Wave Information Studies (WIS) project [21].

2.2.2.1. NOAA Buoys

Measured wave data are available for two active buoys operated by the National Data Buoy Center (NDBC) in Lake Erie: Buoys 45005 and 45009. Buoy 45005 has been in operation since 1980. Buoy 45009 has data for only 7 months in 1983 [22]. In addition, two buoys operated by the Canadian government, Buoys C45132 and C45142, have been recording wave data in northern and northeastern Lake Erie [23]. To avoid potential damage to the buoys, they are usually removed over winter, when the lake is extensively ice-covered. As a result, no wave data are collected during winter. Figure 2(a) shows the locations of these buoys. Table 1 summarizes the geographical coordinates and data inventories of the Lake Erie wave buoys.

Table 1. Wave buoys: Location and data inventory

Buoy Name	Longitude	Latitude	Depth	Record Duration
45009	-82.00	41.60	unknown	06/1983 - 12/1983
45005	-82.40	41.68	12.5	06/1980 - present
C45132	-81.22	42.47	21	09/1989 - present
C45142	42.74	-79.29	27	07/1994 - present

2.2.3. WIS Stations

The WIS data are based on hindcast simulations of wave characteristics. The archived Lake Erie wave data are generated using the spectral wave model WISWAVE. The model solves the energy balance equation and a 2-D wave spectrum, and includes shallow water effects [24,25].The Lake Erie hindcast wave data were produced through the USACE's WIS project, and are available for the periods 1960-1978 and 1979-2014. The data are made available on the WIS website for 243 stations around the lake [21]. Figure 2(b) shows the location and water depth for the WIS stations. The surface ice data were used as input to the WISWAVE model. The lake-wide WISWAVE output for the year of 2011, supplied by the USACE as a representative year for the lake wave climate, are used for wave energy analysis in the following.

Station	92001	92020	92050	92100	92110	92130	92170	92200	92230
Depth (m)	15	38	18	7	6	10	13	60	15

Figure 2. (a) Lake Erie water level gauges (stations) and wave buoys; (b) The 243 wave stations for Lake Erie WIS hindcast (colored balls). Every 10th stations is labeled.

2.2.4. Wind Climate

Figure 3 shows the wind roses for the WIS stations 92001 and 92110 located near Buffalo and Toledo, respectively (see Figure 2). The wind roses are based on the data for 1979-2014. The predominant wind direction is along the longitudinal axis of the lake (at 247.5^0) and can reach up to 25 m/s, near Buffalo at the eastern end of the lake. The predominant wind at the western end of the lake, near Toledo, can reach up to 20 m/s at 225^0 in the clockwise direction from North, slightly different from that at Buffalo.

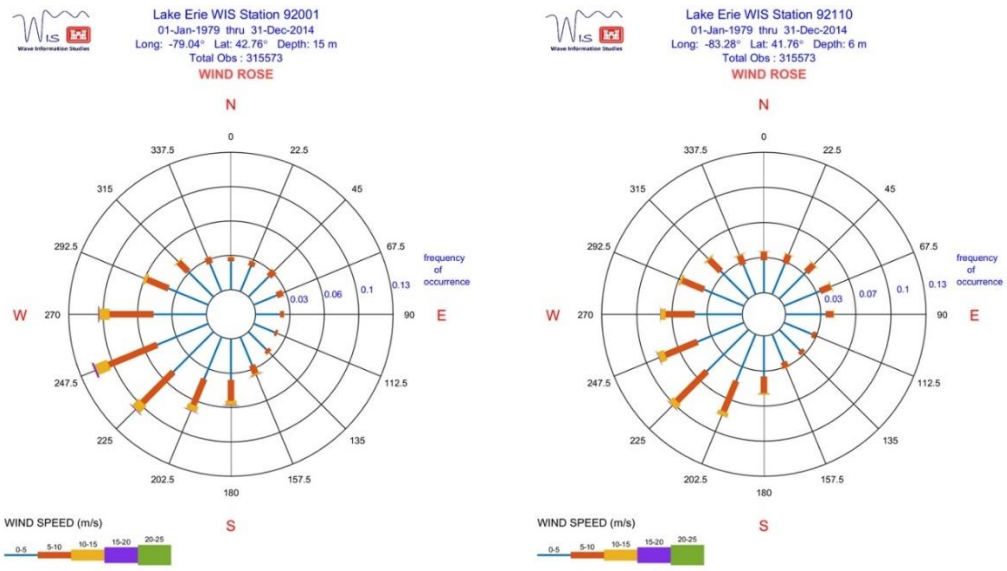

Figure 3. Long-term wind roses for WIS stations 92001 and 92110 [21]

2.2.5. Water Elevation Data

Lake Erie water level variations are recorded at the NOAA [26] and Canada's Department of Fisheries and Oceans [27] water level stations shown in Figure 2. For this study, hourly lake level data from 12 stations are used. Eight stations are operated by NOAA, and four stations operated by the Canadian Government. The location of these stations, and their hourly data inventory, are summarized in Table 2. Hourly data are available for all but one of the stations from 1970 until present, as shown in the table.

Table. 2. Water level stations locations and their data inventory for hourly lake level

Station Name (Station Number)	Longitude	Latitude	Data Period
Buffalo, NY (9063020)	-78.890	42.877	01/01/1970 - present
Erie, PA (9063038)	-80.092	42.153	01/01/1970 - present
Cleveland, OH (9063063)	-81.635	41.540	01/01/1970 - present
Toledo, OH (9063085)	-83.472	41.693	01/01/1970 - present
Fairport, OH (9063053)	-81.280	41.758	06/05/1975 - present
Fermi Power Plant, MI (9063090)	-83.257	41.960	01/01/1970 - present
Gibraltar, MI (9044020)	-83.185	42.090	01/01/1970 - present
Wyandotte, MI (9044030)	-83.147	42.202	01/01/1970 - present
Bar Point, ON (12005)	-83.117	42.050	06/01/1966 - present
Port Stanley, ON (12400)	-81.217	42.667	06/01/1927 - present
Port Dover, ON (12710)	-80.200	42.783	01/01/1962 - present
Port Colborne, ON (12865)	-79.250	42.867	01/01/1962 - present

2.3. Spectral Analysis

To identify and quantify modes and the corresponding energy of Lake Erie's low frequency oscillations (*i.e.* seiches) spectral analysis of the lake's hourly water level data was performed.

Power Spectral Density (PSD), S_{xx}, is defined as the Fourier transform of autocorrelation, $R_{xx}(\tau)$, of a real stationary signal $x(t)$.

$$S_{xx}(f) = \int_{-\infty}^{\infty} R_{xx}(\tau) e^{-2\pi i f \tau} d\tau \tag{1}$$

$$R_{xx}(\tau) = E\left[x(t)x(t+\tau)\right] = \int_{-\infty}^{\infty} S_{xx}(f)e^{2\pi i f\tau}df \quad (2)$$

where *E* denotes the expected value. The spectral analysis method utilized here provides information regarding various low frequency oscillation modes, among which the frequencies corresponding to free oscillations of seiching modes are apparent. The analysis is performed using Lake Erie long-term hourly water level data for various NOAA water level stations around the lake, so that the spatial variations of the seiching modes' frequencies and magnitudes are presented.

2.4. Numerical Modeling

To provide detailed information regarding lake-wide surge, seiche and wave, and the corresponding energy characteristics, numerical models were applied. A coupled circulation and spectral wave model, ADCIRC+SWAN [28], was used to simulate a number of extreme storm events. The coupled model consists of the circulation model, ADCIRC (Advanced Circulation Model, ADCIRC) [29], and spectral wave model, (Simulating WAves Nearshore, SWAN) [30], which are described in the following sub-sections. A wide range of physical data including topographic, bathymetric, atmospheric, water level, wave and ice data were collected, processed and used as input to the lake-wide model. An unstructured lake grid and wind and pressure fields are used as main inputs to the model, Parallel ADCIRC and SWAN (PADCSWAN). The mesh was developed based on seamless Digital Elevation Model (DEM) data of the lake. The seamless DEM is developed from NOAA bathymetry data [31]. The maximum and minimum spacing are set at approximately 500 m and 60 m, respectively. Depths are relative to 174.0 m (The North American Vertical Datum of 1988, NAVD88), the long term average lake level.

The coupled SWAN spectral wave model and the ADCIRC shallow-water circulation model, which is based on an unstructured-mesh, is utilized for the simulation of extreme storms. The two models use an identical mesh, run based on parallel computing mechanism, and exchange information between models during runs. By coupling the wave and surge models, computed radiation stress from SWAN are passed to ADCIRC, and used as additional forcing for water level prediction. The simulated water level is then passed to SWAN as an updated water level for wave modeling. This process takes place at every SWAN model time step. Forcing mechanisms can be wind speed, atmospheric pressure, water level, current, and radiation stress gradients. In this study, the model was forced by the wind and pressure fields, based on the NOAA Climate Forecast System Reanalysis (CFSR) hindcast [32]. Parallel simulations based on domain decomposition embedded in the model reduces the computation time. The unstructured mesh in the integrated SWAN and ADCIRC model allows for spatial variation of resolution without resorting to nested meshes, which could be complex and computationally expensive, particularly if two-way nesting is employed. The coupling can be very important for accurate results for Lake Erie, where storm-induced water level variations can reach up to about ±3 m. Such changes of depth in shallow regions can significantly influence wave characteristics which could, in turn, impact water level through wave setup. These processes would not be included if wave and storm surge were modeled independently. More details about the ADCIRC and SWAN models, including their settings, are provided in the following sections.

2.4.1. ADCIRC model

ADCIRC is a finite-element, shallow-water model for water level and current. Water level is predicted by solving the Generalized Wave Continuity Equation (GWCE), based on the vertically-integrated continuity equation [29].

$$\frac{\partial H}{\partial t} + \frac{\partial}{\partial x}(UH) + \frac{\partial}{\partial y}(VH) = 0 \quad (3)$$

where $U, V =$ depth-averaged velocities in *x,y* directions; $H = \eta + h$ = total water column thickness; *h* = bathymetric depth (distance from the geiod to the bottom); η = free surface departure from the geoid.

ADCIRC solves the vertically-integrated momentum equations to determine the depth-averaged velocity. The vertically-integrated momentum equations can be written in non-conservative form.

$$\frac{\partial U}{\partial t}+U\frac{\partial U}{\partial x}+V\frac{\partial U}{\partial y}-fV=-g\frac{\partial\left[\eta+P_s/g\rho_0-\alpha\varsigma\right]}{\partial x}+\frac{\tau_{sx}}{H\rho_0}-\frac{\tau_{bx}}{H\rho_0}+\frac{M_x}{H}-\frac{D_x}{H}-\frac{B_x}{H}$$
$$\frac{\partial V}{\partial t}+U\frac{\partial V}{\partial x}+V\frac{\partial V}{\partial y}+fU=-g\frac{\partial\left[\eta+P_s/g\rho_0-\alpha\varsigma\right]}{\partial y}+\frac{\tau_{sy}}{H\rho_0}-\frac{\tau_{by}}{H\rho_0}+\frac{M_y}{H}-\frac{D_y}{H}-\frac{B_y}{H} \quad (4)$$

where f = Coriolis parameter; P_s = atmospheric pressure at the sea surface; ς = Newtonian equilibrium tide potential; τ_{sx} ,τ_{sy} = imposed surface stresses; τ_{bx},τ_{by} = bottom stress components; D_x, D_y = momentum dispersion; M_x, M_y = vertically-integrated lateral stress gradient; B_x,B_y = vertically-integrated baroclinic pressure gradient; ρ = time and spatially varying density of water due to salinity and temperature variations; ρ_o = reference density of water.

ADCIRC computes water level η and current U and V on an unstructured, triangular mesh by applying a linear Lagrange interpolation and solving for three degrees of freedom at every mesh vertex.

A number of nodal attributes were used as input to the model [33]. The initial offset of sea surface from the geoid (sea surface height above geoid) for the initial lake level is assigned to the mesh nodes. This offset is based on the mean lake level at the beginning of a storm. The Manning's friction factor (mannings *n* at sea floor) nodal attribute is calculated using the standard routine from the ADCIRC website. This nodal attribute is determined according to Land Use and Land Cover (LULC) data from the National Land Cover Data (NLCD [34]). The "primitive weighting in continuity equation" attribute, a factor that weighs relative contribution of primitive and wave portions of the Generalized Wave-Continuity Equation is generated based on the model mesh. The "surface directional effective roughness length" attribute representing "roughness" of land that can reduce wind-induced surface stress is calculated based on the LULC data. The "surface canopy coefficient" attribute allowing to turn off wind stress in inundated heavily forested areas is determined using the standard routine from the ADCIRC website, based on the LULC data. No tidal constituents are introduced to the model, since tides are insignificant in the Great Lakes. The computational time step for ADCIRC is set to 1 s.

2.4.2. SWAN model

The SWAN model simulates wave action density spectrum N (x, t, ω, θ) by solving the action balance equation [30].

$$\frac{\partial N}{\partial t}+\nabla\left[\left(\vec{C}_g+\vec{U}\right)N\right]+\frac{\partial C_\theta N}{\partial\theta}+\frac{\partial C_\omega N}{\partial\omega}=\frac{S}{\omega} \quad (5)$$

where ∇ = gradient operator; $\vec{C}_g$ = group velocity vector; C_θ = turning rate; C_ω = shifting rate; $\vec{U}$ = current vector; S = source terms; ω = relative frequency; and θ = wave direction.

The wave action density spectrum N is solved at the vertices of unstructured triangular mesh. The model represents physical processes at scales of a wave length, even if mesh resolution is higher than the wave length. The Komen et al. (1984) wave generation with linear growth (Cavaleri and Malanotte-Rizzoli, 1981) was activated. Whitecapping was applied according to Komen et al. (1984) with the default coefficients [30]. The SWAN model time step is set to 1,800 s, which is also the time step at which the ADCIRC and SWAN models exchange information.

2.4.3. Surface Ice Effects

Surface ice can modify storm surge and wave characteristics, mainly through wind-lake momentum transfer mechanism. Nearshore or shore-fast ice can hinder waves from reaching the shoreline. To incorporate ice effects in storm surge prediction processes, the wind drag coefficient needs to be

modified. In the absence of ice, the ADCIRC model uses Garratt's empirical wind drag, C_{DN}, which is capped at 0.0035 [35].

$$C_{DN} = (0.75 + 0.067\, U_{10})\, 10^{-3} \tag{6}$$

where U_{10} is 10 m elevation above ground wind speed.
The wind drag coefficient is determined as the larger of drag coefficient based on Garratt's formula and that based on the ice-percentage-dependent formulation, C_{DF} [36]. The latter was developed based on an empirical fit to field data for ice concentration and air-ice-water wind drag coefficient [37,38].

$$C_{DF} = [0.125 + 0.5\, IC\, (1.0 - IC)]\, 10^{-2} \tag{7}$$

where IC is percentage ice cover or ice concentration, (IC = 0 and IC = 1 represent ice-free and ice-covered conditions, respectively) [39].

In the ADCIRC model, C_{DF}, is compared with C_{DN}, and the larger value is taken as the drag coefficient used for calculation of wind-induced surface stresses at any time-step. According to Eq. 7, the drag coefficient which is a function of both ice concentration and wind speed reaches its maximum when ice concentration is at 50 percent, and approaches Garratt's drag formulation for concentrations of 0 and 100 percent. Further investigation of the surface ice effects on the Lake Erie storm surge confirmed that the surface ice effects on storm surge is more pronounced at lower wind speeds and modest ice concentration [40].

To include surface ice effects in the wave model, wave height is simply set to zero when ice concentration exceeds a threshold value. In this study, the ice concentration threshold is set to 70%, a value adopted from the studies in the western Alaska waters [41]. The WIS project adopts the same threshold for wave simulations.

2.5. Formulation of Wave and Seiche Energy in a Lake

Wind generates seiche and surface waves in a lake. The seiche energy is in the form of potential energy, and can be evaluated at any point in time as follows

$$E_s(t) = \int gzdm = \int \rho g z\, dv \tag{8}$$

where m is mass, g is the gravitational acceleration, z is elevation above a datum, and v is volume. When a lake is discretized into a number of elements or cells using a numerical model, the seiche energy can be estimated by summing the potential energy of each element/cell as follows

$$E_s(t) = \sum g\, \bar{\eta} \delta\, m = \frac{1}{2} \sum g \rho\, \eta |\eta| \delta\, A \tag{9}$$

where η is the water elevation above the still water level (SWL; no seiche). The absolute sign indicates that the potential energy is negative for elements/cells that have negative surge (*i.e.*, water level below SWL) and positive for elements with positive surge. The total seiche energy of a lake after a wind event gradually decreases over time by energy dissipation.

The potential energy of a seiche can be theoretically harvested by a similar concept used in tidal lagoons (*e.g.*, [42]). The main period of seiche is about 14 hours (see the results section), which is close to that of semi-diurnal tide (about 12 hrs). In other words, the oscillation of water level by seiche is similar to a semi-diurnal tide in Lake Erie. Referring to Figure 4, a barrier can create a phase lag between the water level inside the lagoon and the lake. Gates are initially left open. When water reaches its maximum level during a surge event, the gates of the lagoon are closed. The water level outside the lagoon decreases over time, while the water elevation inside the lagoon remains constant. This leads to a head over turbines. When enough head is available, the generators start operating, until the surge returns and the head is no longer sufficient to drive the turbines.

The power generated by this method is proportional to the area of the lagoon and the square of the head [43]. The power during a seiche cycle when turbines operate (*i.e.* from t_1 to t_2) can be evaluated as

$$E_p = C_p \int_{t_2}^{t_1} \rho g \, A_p \, \frac{dh_p}{dt} \, (h_p - h_L) \, dt \tag{10}$$

where A_p is the area of lagoon, h_p is the water elevation inside the lagoon, and h_L is water elevation outside the lagoon. C_p is the power coefficient, and takes into account the efficiency of the turbines and energy losses.

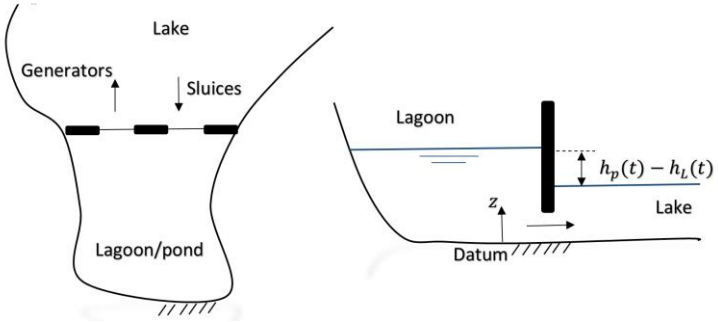

Figure 4. Schematic of a tidal lagoon to trap and harvest seiche energy by creating a phase lag between water elevation inside and outside of a lagoon

The main technical challenge of generating electricity by this method is finding a turbine which can work efficiently for the values of head during a seiche event, which are relatively small. Here, we aim at evaluating the energy of seiche, which may not be possible to harvest at the moment by current turbine technology, but it will demonstrate the potential for the future.
The wave power, for irregular waves, which have a range of frequencies and directions, can be computed as

$$P = \iint c_g E(\theta, \sigma) \, d\sigma d\theta \tag{11}$$

where c_g is the group velocity, and *E* is wave energy density. In many cases, deep water approximation gives a reasonable estimate for wave energy resource assessments. For this case ($kh \geq \pi$ where *k* is wave number and *h* is water depth), the wave energy can be estimated as

$$P = \frac{\rho g}{64\pi} \, H_s^2 T_e \tag{12}$$

where H_s is the significant wave height, and T_e is the energy wave period. Both of these wave properties can be evaluated by the wave spectrum [44].

3. RESULTS

In the following sections, the results of the data analyses and numerical modeling are presented.

3.1. Storm Surge, Seiche and Wave Climate of Lake Erie

Lake Erie hourly water level time-series at various stations were analyzed to identify and quantify the spatial variations of extreme surge and seiche events. Likewise, the hourly wave data from the NDBC buoy and WIS stations were analyzed.

3.1.1. Storm Surge

In order to identify and quantify the storm surge events, the hourly data was subtracted from its mean over a 30-day time window. The averaging is performed using a moving average method that employs a Gaussian algorithm for smoothing. Figure 5 depicts the hourly and the averaged water level elevations

(top). The deviation of the instantaneous water level from its monthly mean value (*i.e.*, storm surge) is plotted in the lower panel.

3.1.2. Extreme Surge Events

To identify extreme surge events based on the 'Peaks Over Threshold (POT)' method, any events exceeding a sufficiently high threshold are categorized as extreme events. To avoid selecting multiple peaks during a single storm, a 48-h span is considered for each storm, and only one event is selected during that time-frame. Selecting an appropriate value as the threshold surge is important. In samples taken from normal or extreme value populations, best results are obtained if the threshold is chosen so that the number of exceedances is of the order of ten per year [45]. The threshold is chosen as the mean surge level plus three times the standard deviation of the surge. Sensitivity analysis showed that the selected threshold value is the best value for Lake Erie.

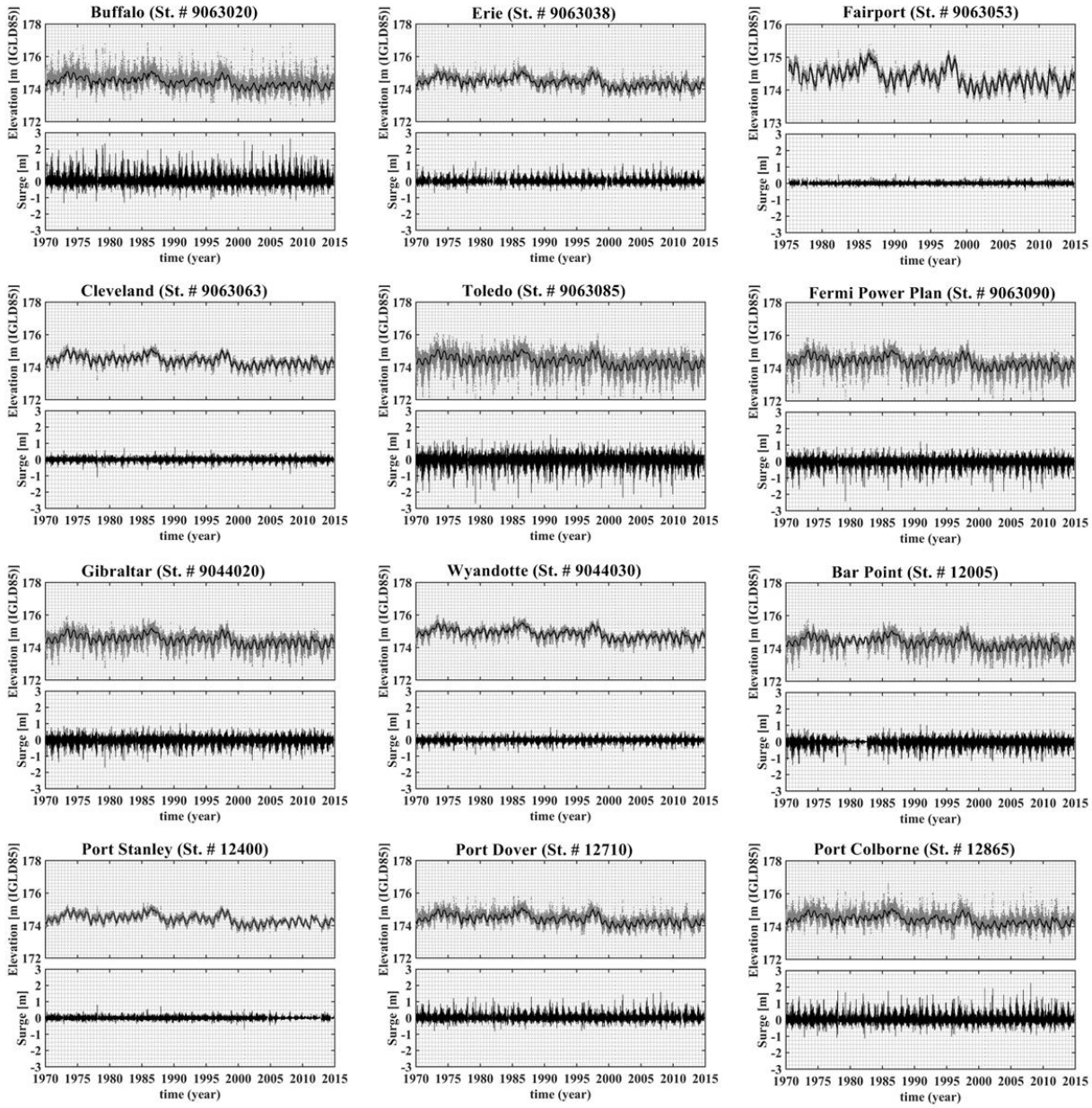

Figure 5. Hourly water level and surge timeseries at various stations for duration of 46 Years; Upper panel: hourly water level, gray dots: instantaneous; dark line: smoothed; Lower panel: storm surge

The largest storm surges were identified for each water level station. Figure 6(a) shows the top 20 historical storms, and the corresponding measured surges for Buffalo and Toledo where surge levels are typically larger. Storm surges are typically larger in Buffalo than Toledo primarily because of the predominant wind direction, which is in the west-east direction. The storm surge in parts of eastern Lake Erie can reach up to nearly 3.0 m.

Figure 6(b) shows the typical distribution of extreme storm surge events for Buffalo and Toledo during 2013, selected as an example. As Figure 6(b) shows, most of the storms take place during November-May. However, the majority of extreme events occur in late-fall and during winter.

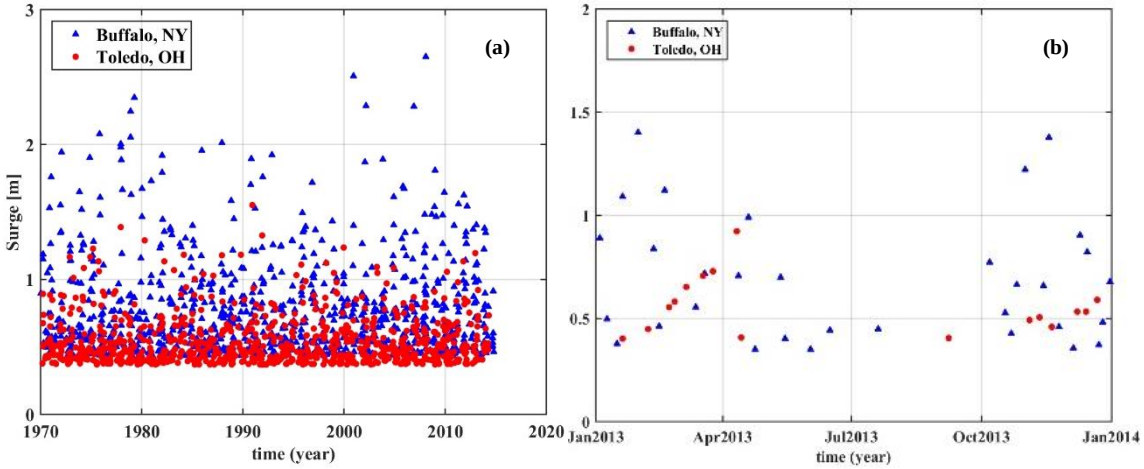

Figure 6. (a) Top 20 historical extreme events per year for Toledo and Buffalo; (b) Distribution of extreme events for Buffalo and Toledo during 2013

The surge events for each water level monitoring gauge in Lake Erie were identified using the POT method. The return period analysis was then conducted for the selected storm surges at each gauge by fitting four different distributions: Generalized Pareto Distribution (GPD), Lognormal, Weibull, and General Extreme Value (GEV). The average number of storms per year is λ=10 as this value produces the best fit for the present data. Figure 7 displays the extreme storm surge distributions against the return periods for the best fitted distribution, GPD, for the 12 stations. Based on the results, the most severe storm surges occur on the eastern side of the lake. Table 3 summarizes the results of the return period analysis of wave height depicted in Figure 7. The 500-year surge elevation in Buffalo is forecasted as 3.3 m. The west side of the lake is also vulnerable to the high surge; however the 500-year storm surge in Toledo is expected to be 1.8 m. The lowest storm surge elevations are predicted to occur in areas around the middle of the lake's longitudinal axis (*e.g.*, Fairport and Cleveland in the south shore, and Port Stanley on the north shore). Wyandotte is located upstream of Detroit River from its mouth in Lake Erie. Table 3 summarizes the surge heights for various return periods based on the GPD method.

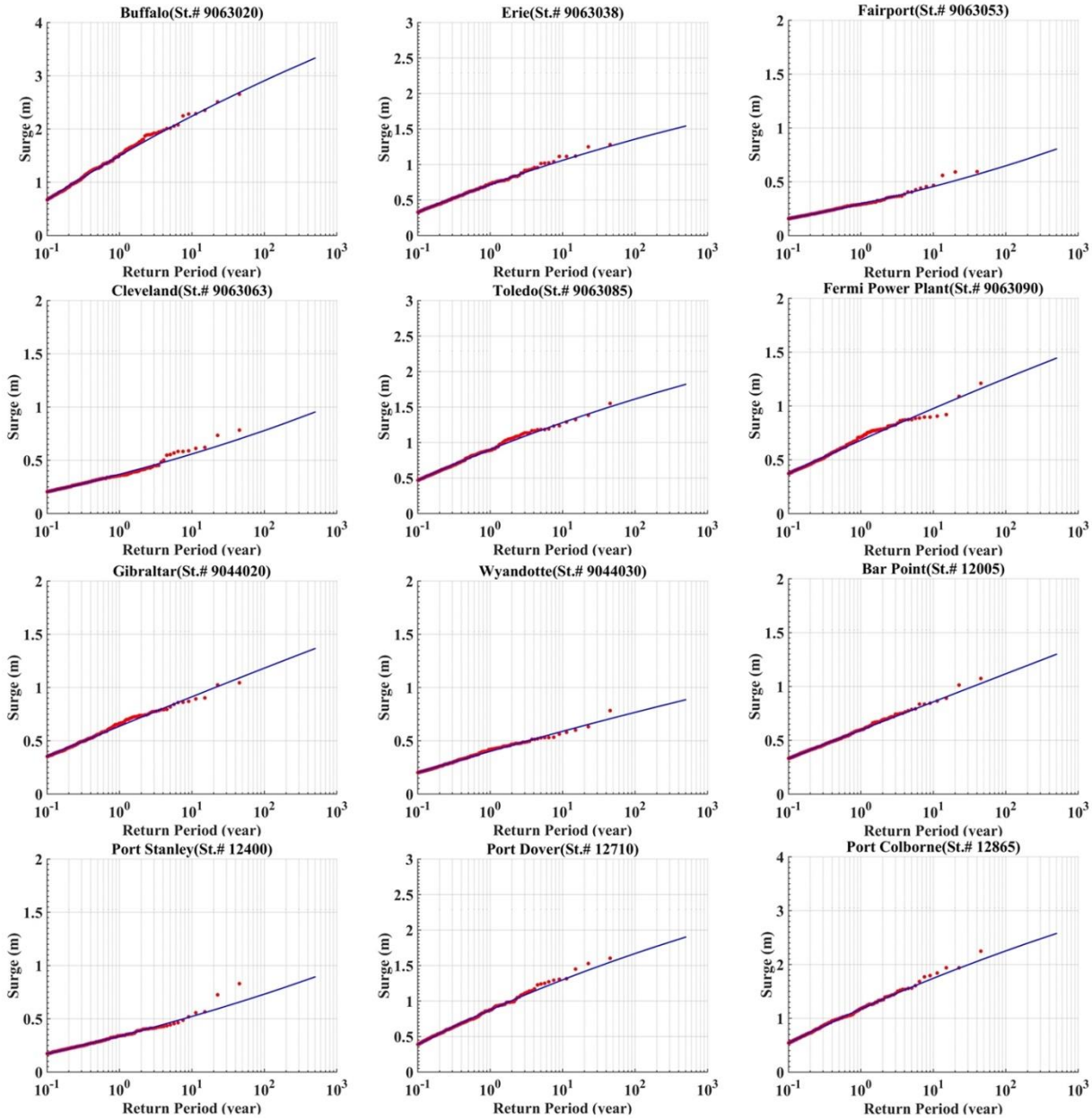

Figure 7. Storm surge vs. return period based on GPD for selected stations

Table 3. Surge elevation for various return periods

	Return Period (year)			
Station Name (Number)	**100**	**150**	**200**	**500**
Buffalo, NY (9063020)	2.91	3.02	3.10	3.33
Erie, PA (9063038)	1.36	1.41	1.44	1.54
Fairport, OH (9063053)	0.65	0.69	0.71	0.80
Cleveland, OH (9063063)	0.78	0.82	0.85	0.95
Toledo, OH (9063085)	1.61	1.67	1.70	1.82
Fermi Power Plant, MI (9063090)	1.26	1.30	1.34	1.44
Gibraltar, MI (9044020)	1.18	1.23	1.26	1.37
Wyandotte, MI (9044030)	0.77	0.80	0.82	0.89
Bar Point, ON (12005)	1.12	1.16	1.20	1.30
Port Stanley, ON (12400)	0.73	0.77	0.80	0.89
Port Dover, ON (12710)	1.67	1.73	1.77	1.90
Port Colborne, ON (12865)	2.25	2.34	2.40	2.58

3.1.3. Seiche

Figure 8 shows the spectra of the long-term data at selected stations. The spectral energy corresponding to the frequencies up to 8 (cycles/day) are shown in this figure. A band pass filter is used to filter out oscillations with periods of longer than two weeks and shorter than 2.5 hours, as they are considered to be beyond the storm-induced seiching modes. According to Figure 8, several distinct spikes at frequencies of 1, 1.7, 1.9, 2.6, 4.1 and 5.8 (cycles/day) are identified. Those frequencies are equivalent to periods of 24, 14.2, 12.4, 9.2, 6, 4.1 hours. The periods of 24 and 12.4 hours correspond to diurnal and semidiurnal lake level fluctuations, respectively [11]. The periods of 14.2, 9.2, 6 and 4.1 are related to the first four modes of oscillations of seiches [17]. At Buffalo and Toledo, the low frequency motions are more energetic than the other stations. Toward the middle of the lake (a node for the first mode of seiching oscillations) the energy spectra are characterized by lower energy.

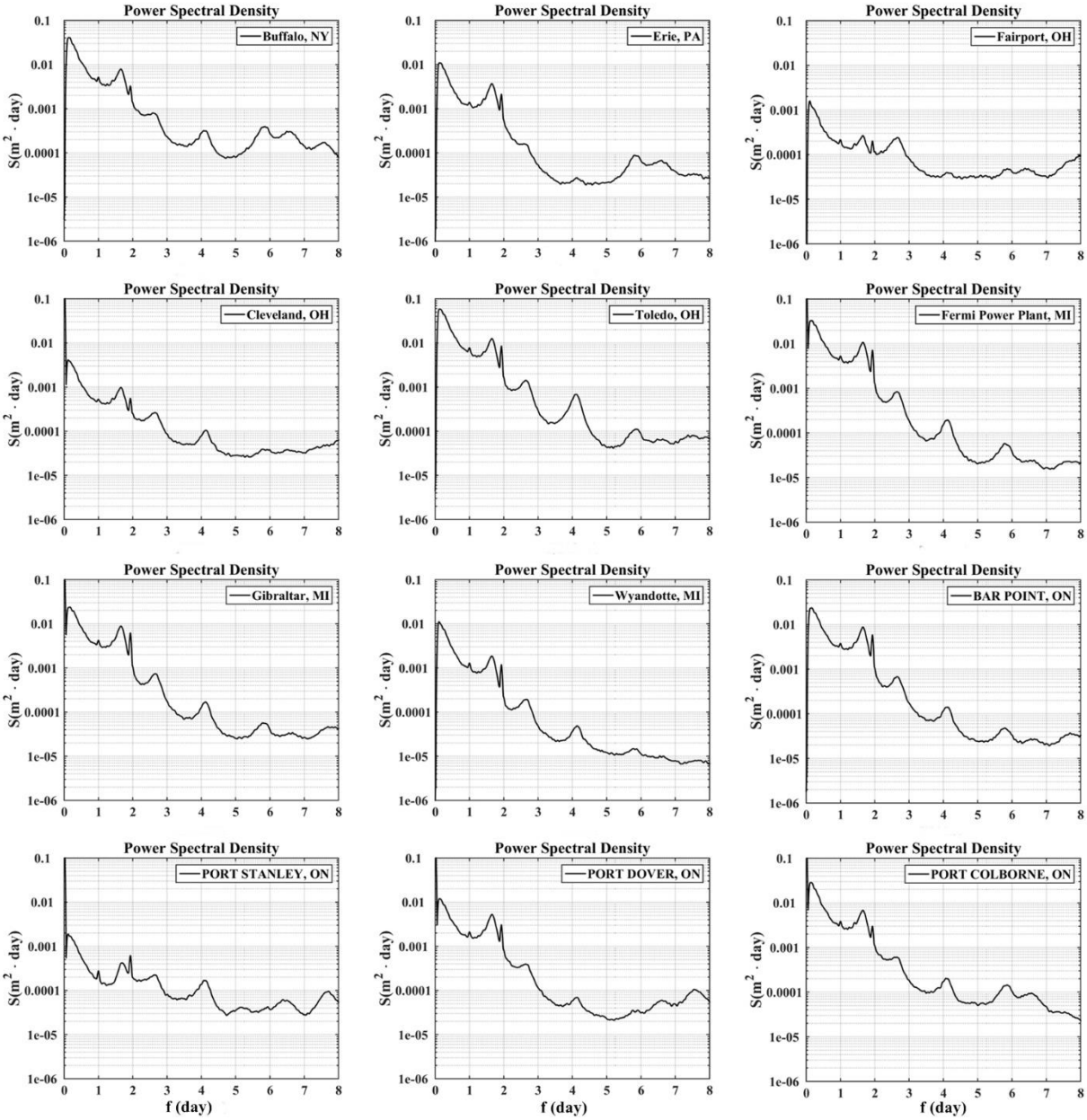

Figure 8. Spectra of Lake Erie long-term water level for selected stations

3.1.4. Analysis of Wave Data

Wave data include data from three NDBC buoys, in addition to nine selected WIS stations.

3.1.4.1. Buoys

As noted earlier, wave data include data from three wave buoys and the USACE's hindcast wind, WIS (see Figure 2). Hourly wave data from the three active buoys, C45132 and C45142 and 45005, were analyzed to quantify magnitudes of wave heights for various return periods. Similar to the water level analysis, POT method was used to identify extreme wave events. Then, the four aforementioned probability distribution methods were used, out of which the GPD was found to provide the best fit to the wave. Figure 9 shows the return period analysis of the wave data for the three buoys. The largest waves are expected to occur in the eastern basin, the deepest basin with the longest fetch, where C145142 operates, the C145132 in the central basin, and finally Buoy 45005 in the western basin where water

depth is relatively shallow and the fetch is short. The 100-year significant wave heights for C45142, C45132 and 45005 are 5.65 m, 4.51 m and 3.75 m, respectively.

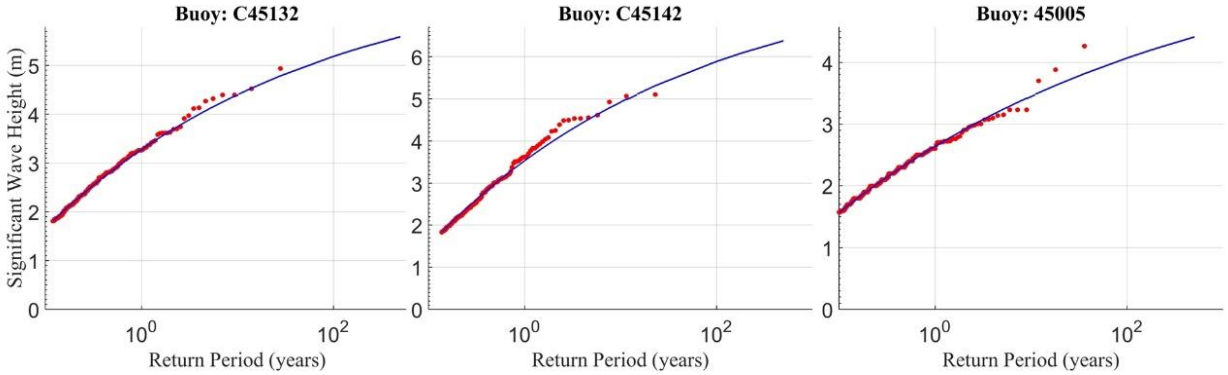

Figure 9. Wave height distribution vs. return period for buoy data using GPD

Table 4 summarizes the results for various return periods.

Table 4. Wave height for various return period for wave buoys using GPD

	Station ID		
	45005	C45132	C45142
Return Period (year)	Significant Wave Height, H_s (m)		
500	3.97	4.73	6.08
200	3.85	4.62	5.85
150	3.81	4.58	5.77
100	3.75	4.51	5.65
50	3.61	4.39	5.40

3.1.4.2. WIS Stations

The WIS data for nine stations that represent the wave climate around the lake were analyzed. The locations of the WIS stations and the corresponding water depths are shown in Figure 2. The GPD was found to provide the best fit to the WIS data. Table 5 summarizes the results for the return periods of 100, 150, 200, and 500-year based on the GPD method. Larger waves occur in the eastern basin, due to the presence of longer fetches and deeper water.

Table 5. Wave height vs. return period for selected WIS stations using GPD

	Return Period (year)			
Station Number	**100**	**150**	**200**	**500**
92001	6.23	6.36	6.45	6.7
92020	7.18	7.25	7.29	7.41
92050	5.64	5.72	5.77	5.92
92100	3.01	3.09	3.15	3.31
92110	2.64	2.73	2.79	2.99
92130	3.78	3.87	3.94	4.14
92170	5.57	5.68	5.75	5.96
92200	7.81	7.89	7.95	8.09
92230	6.33	6.41	6.46	6.60

3.2. Coupled ADCIRC-SWAN Model Results

In the following, the coupled storm surge and wave model results are presented for two extreme events, the storms of January 30, 2008 and December 12, 2000.

3.2.1. Ice Field

The ice field data are provided to the model as spatially and temporally varying concentration fields. The daily ice fields are generated by interpolating the NOAA ice data and used as input to the model when the lake is ice-covered. Figure 10 and Figure 11 show the input ice fields during storms of January 30, 2008 and December 12, 2000.

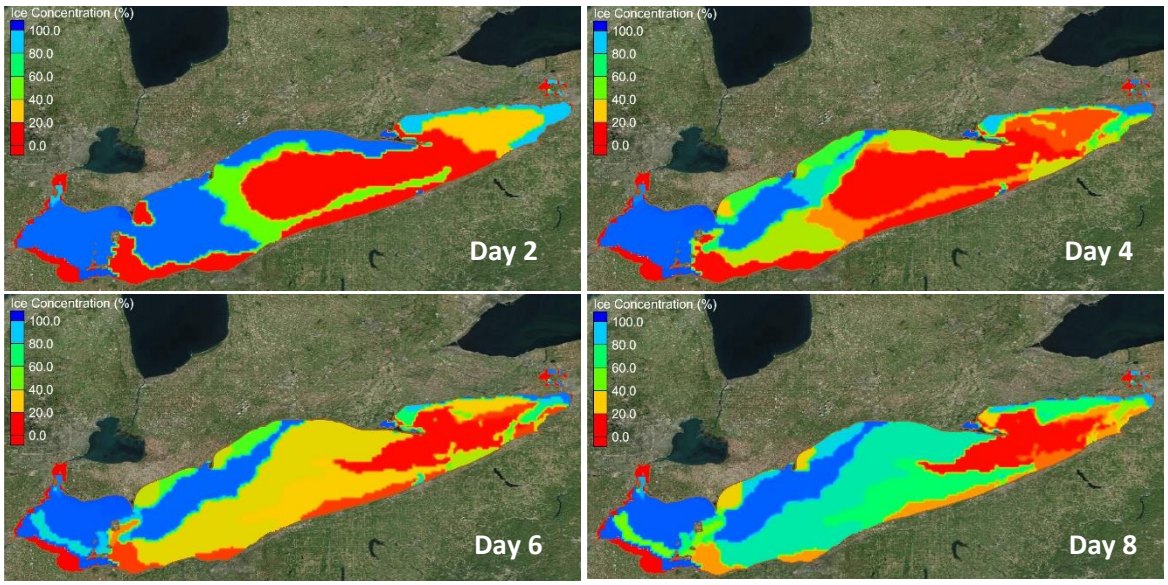

Figure 10. Ice Field during storm of January 30, 2008 (day 1: 01/27/2008)

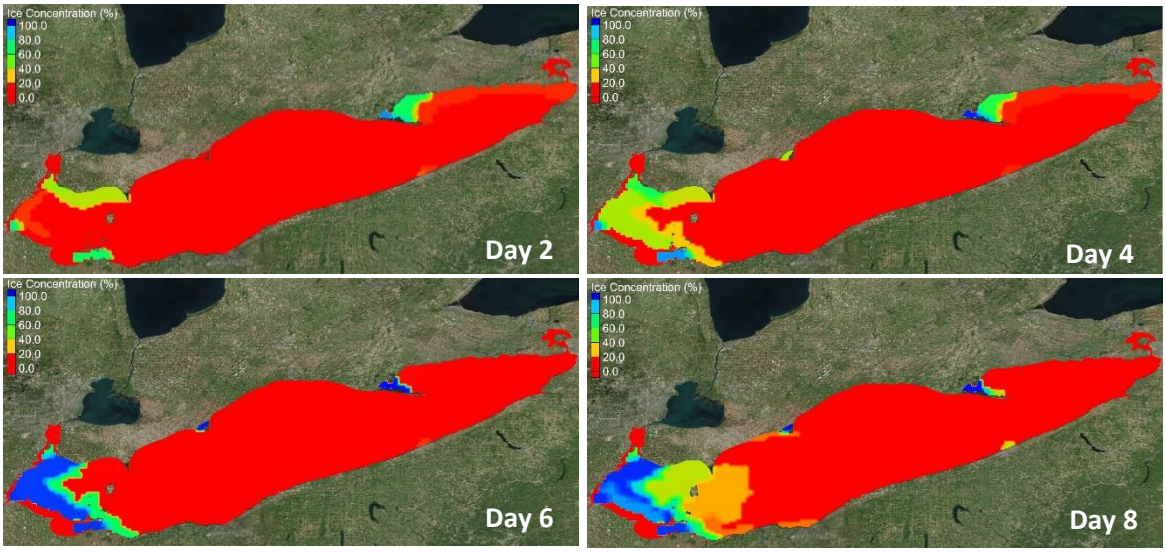

Figure 11. Ice field during storm of December 12, 2000 (day 1: 12/09/2000)

3.2.2. Wind Fields

Winds are typically westerly in the study area, resulting in higher storm surge in eastern Lake Erie. Figure 12 shows the wind fields during the peaks of storms of January 30, 2008 and December 12, 2000, when the maximum hourly wind speed over Lake Erie reached almost 25 m/s.

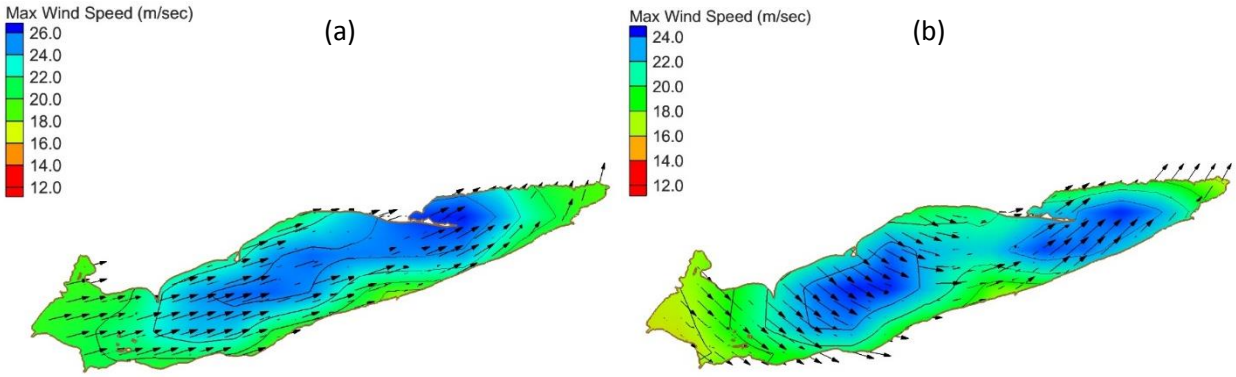

Figure 12. Maximum wind speed during storms of: (a) January 30, 2008; (b) December 12, 2000

3.2.3. Model Validation

Two extreme events, the storms of January 30, 2008 and December 12, 2000, were simulated using the coupled ADCIRC+SWAN modelling system. The former storm took place when the lake was extensively ice-covered. The latter storm occurred under relatively minor surface ice condition. Both storms led to significant storm surges in eastern Lake Erie.

To simulate the two extreme events, wind and pressure fields were introduced as forcing input to the model. The threshold ice concentration of 70% is adopted for this study, as explained earlier. Figure 13 and Figure 14 show the comparisons of storm surge variations at different stations for the storms of January 30, 2008 and December 12, 2000, respectively. As the figures show, during the peak of the storms, areas close to Buffalo and Erie on the east undergo high storm surges while at the western end of the lake, near Cleveland and Toledo, the lake level falls. The model captures the temporal variation and magnitude of the surge at various stations. This is quantified in the right panels using Root-Mean-Square Error (RMSE) for the model results compared to the measured water level. The maximum storm surge level in Buffalo reaches nearly 3 m and 2.7 m for the storms of January 30, 2008 and December 12, 2000, respectively. The magnitudes of set-down reach approximately -2.5 and -1.5 m (for the two storms, respectively) at Toledo. The variation of water level is the least at Fairport, located around the middle of the lake's longitudinal axis, and hence a node for the first mode of seiching.

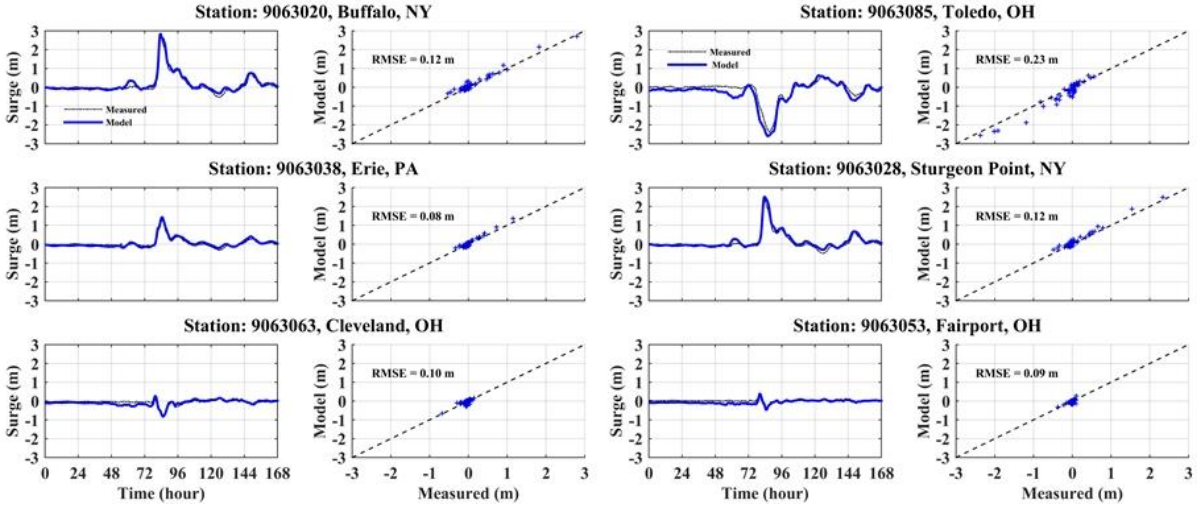

Figure 13. Comparison of simulated and measured water level variations, storm of January 30, 2008

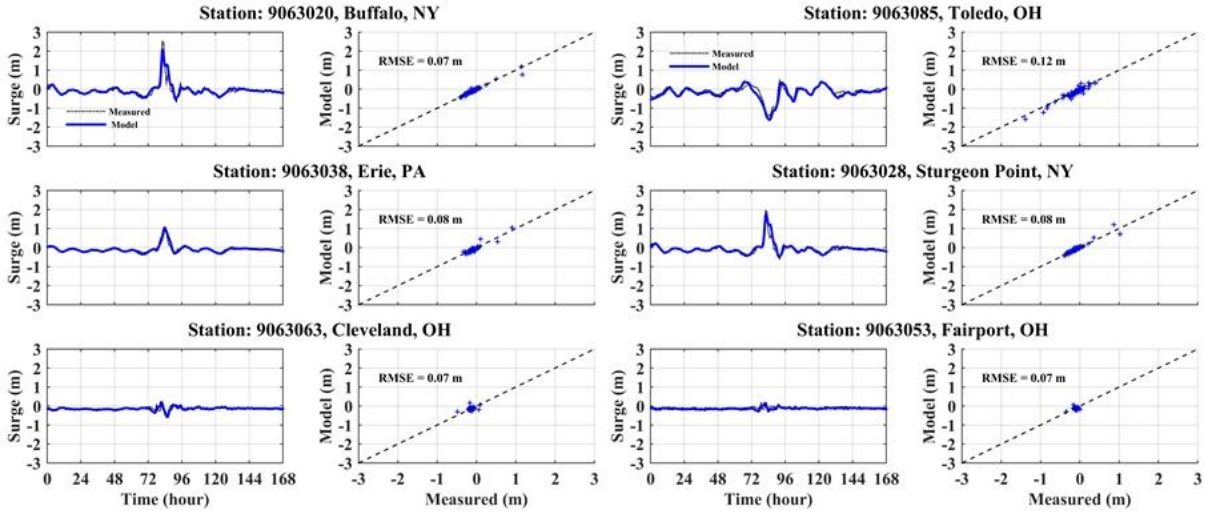

Figure 14. Comparison of simulated and measured water level variations, storm of December 12, 2000

3.2.4. Surge and Wave Energy Assessment

The upper panel of Figure 15 shows the spatial variation of the storm surge during the peak of the storm on January 30, 2008. The lower panel shows the gradient of lake level along the lake's longitudinal axis. The surge almost linearly decreases from +3 m above still water level at the eastern end to approximately -2.7 m at the western end. Such a difference in lake level over a length of approximately 400 km results in a gradient of 1.43×10^{-5}. The spatial variation of the theoretical gravitational potential energy density corresponding to the lake level gradient is estimated and shown in Figure 16. As the figure shows, the maximum energy density is higher on the western and eastern end, and is reduced toward the middle of the lake where the surge is small. The theoretical potential energy in the lake is calculated using Eq. 9. It is estimated that the total energy of the storm of January 30, 2008 is PE = 1.8×10^{5} GJ equal to 5×10^{7} kWh. Although challenging, such energy could be harnessed using a structure such as a surge lagoon, where the head difference between the inside and outside of the lagoon could drive turbines and generate power. In view of this concept, a hypothetical lagoon with an area of A = 2 km^2 is sited near Buffalo, as shown in pink in Figure 16, and the theoretical potential energy (assuming 100% efficiency) that such a feature can capture is estimated as 84 GJ, which is equivalent to 2.3×10^{4} kWh. Considering the average monthly electrical energy usage per home in the State of New York is 591kWh, based on the 2014 estimates [1], the lagoon can supply power equivalent to nearly 40 homes for a month using the surge or seiche energy for this single event. The total surge energy of this storm (5×10^{7} kWh) could, theoretically, power 7,050 homes for a year. A larger lagoon or multiple lagoons could therefore capture more energy from the extreme surge events. Furthermore, the lagoon could reduce flood risk by routing the surge elevation.

Similarly, the results of the storm surge simulation for the storm of December 12, 2000 were analyzed, and the potential seiche energy of the lake and the lagoon estimated. The surge varies from +2 m to -2 m from eastern end to western end, respectively. The surge total potential energy of the storm is estimated as PE = 8.2×10^{4} GJ which is equivalent to 2.3×10^{7} kWh. The lagoon will hold a potential power energy of PE = 45.6 GJ equal to 1.3×10^{4} kWh enough energy to power 22 homes for a month.

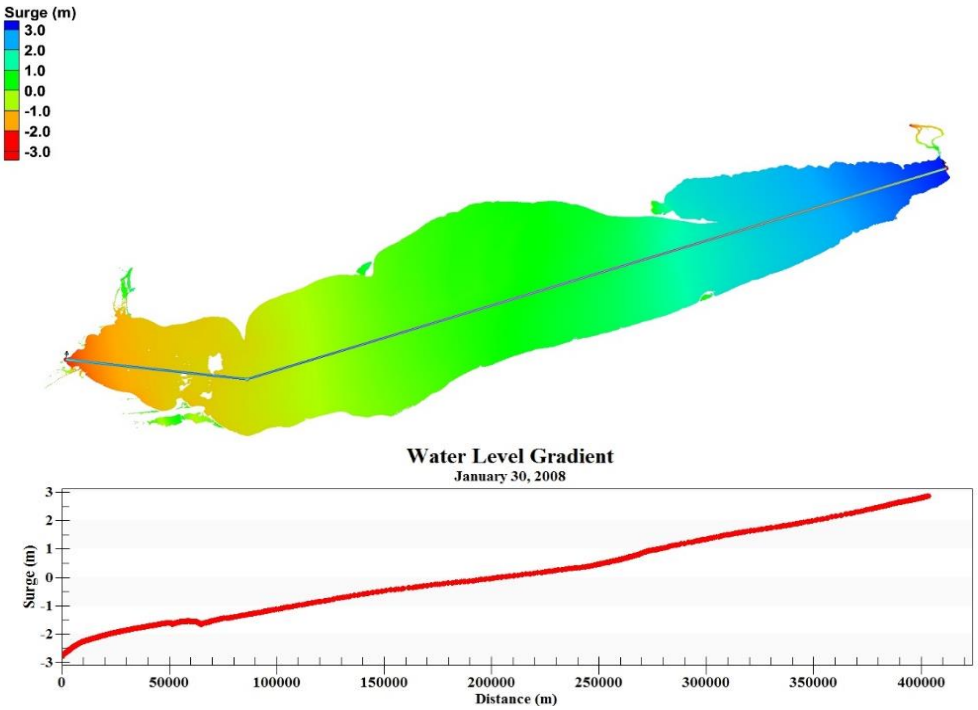

Figure 15. Peak storm surge and gradient of water level during storm of January 30, 2008

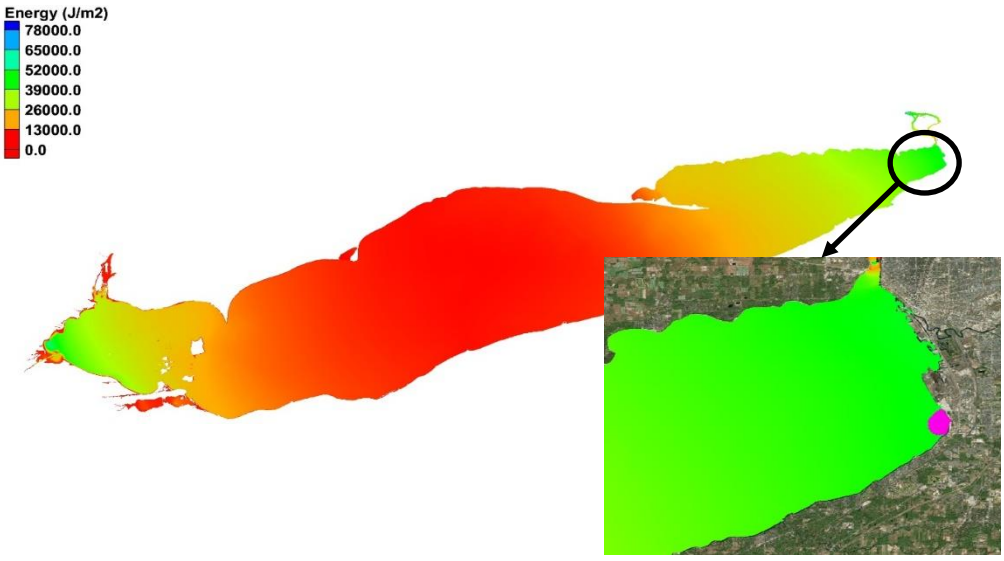

Figure 16. Spatial variation of potential surge energy density during peak of storm, January 30, 2008

3.2.5. Wave Power

As noted earlier, Lake Erie wave data are provided by the USACE. The data are generated as part of the WIS project. A threshold value of 70% is used for ice concentration. Any waves in areas with an ice concentration of 70% or higher are blocked. For this study, the year 2011 is selected. In the winter of 2011, Lake Erie ice cover reached more than 90% of the lake area, a typical ice condition for the lake. The monthly mean significant wave height and peak wave period are calculated based on the hourly wave data. The theoretical wave power, P_w, is calculated based on Eq. 11.

Figure 17 shows the monthly mean spectral wave height, peak period and power for January 2011, when ice cover was limited to the western basin. The largest waves are concentrated in the eastern basin, where the monthly mean wave height was of order 1 m. As a result, the monthly mean wave power is at its maximum in the eastern basin, where the power is of order 4 kW/m.

Figure 18 and Figure 19 show the mean wave power during the periods of January-June and July-December 2011, respectively. During February and March, only a small area in the west of Lake Erie was relatively ice-free. The wave height and power, as expected, are small. In April, when the lake becomes ice-free, a large portion of the lake with relatively deeper water compared to the western basin shows wave power of up to 7 kW/m. The monthly mean wave power in May is reduced to 2.5 kW/m. The wave power remains low during subsequent months as the lake is relatively quiescent in late spring and in the summer. Beginning September, wave power in the lake begins to increase. The mean monthly wave power in September reaches up to 4 kW/m, concentrated in the central part of the lake. The power continues to increase during fall. In October, the monthly mean wave power exceeds 10kW/m in central and eastern parts of the lake. Similar wave power can also be seen during November. In December, the wave power is slightly reduced to 7 kW/m. The area with the highest wave power concentration is on the eastern portions of the lake.

Figure 20 shows the long-term wave characteristics and energy for Buoys C45132, C45142 and 45005. Buoy 45005 is located in an area with relatively shallow depth (12.5 m depth - see Table 1). In addition, the fetch is shorter for this buoy compared to the other two because the predominant wind blows from west toward east. The maximum hourly wave height and corresponding power for some events reaches up to 4 m and 60 kW/m, respectively. Buoy C45132, which is located in an area that is 20 m deep and with longer fetch, shows larger waves compared to Buoy 45005. The maximum hourly wave heights can exceed 4 m during some extreme events. Such waves are associated with hourly power of up to 80 kW/m. Buoy C45142, located further east with a much longer fetch and in deeper water, exhibits maximum hourly wave heights of over 5 m. The maximum hourly wave power for some events exceeds 125 kW/m. The gaps in the data are related to the lack of data during winters because of the lake's surface ice. This would result in a relatively low annual mean wave power.

4. DISCUSSION AND CONCLUSIONS

Characteristics of Lake Erie, including its wave, water level and surface ice fields, were presented. Water level data were analyzed, and the magnitude of storm surge events and their spatial distribution presented. It was demonstrated that high surge levels occur frequently in eastern and western Lake Erie. Such high surge can trigger seiching motions in the lake. The potential for generating power from such a phenomenon was assessed through numerical modeling of individual storm surge events. The potential energy contained in the individual extreme events was calculated. In general, characterizing the marine energy resource of a region involves three stages: theoretical, technical, and practical resource assessment. In the theoretical resource assessment studies, it is assumed that all energy can be harvested 100% efficiency is assumed while in the technical resource assessments, a suitable energy device with a power curve at a particular place is considered. In the practical resource assessments, other constraints such as environmental, navigation, and tourism should be included which may lead to a drastic reduction of the available resource.

It is shown that surge energy, if efficiently harnessed, can potentially provide a significant amount of electricity. It is suggested that features such as surge lagoons could be used to not only provide energy from surge events, but also to provide protection from coastal flooding. The cost of a lagoon could be partially offset by the potential of such a structure, and the operation of the lagoon, to help alleviate flooding during extreme events.

Lake Erie's waves were also analyzed to assess their potential for electricity production. Surface ice cover limits the wave energy potential in winter. During the summer, waves are relatively small. The most

energetic months appear to be September through December. Waves are the more energetic in the central and eastern parts of the lake.

It was shown that during the peak of storm of January 30, 2008, when the surge almost linearly decreases from +3 m above still water level at the eastern end to approximately -2.7 m at the western end, the total theoretical potential energy in the lake is approximately 5×10^7 kWh. If such energy could practically be harnessed using a surge lagoon with a surface area of 2 km^2 near Buffalo, the potential energy of 2.3×10^4 kWh could supply power to the equivalent of 40 homes for a month. The total surge energy of this storm (5×10^7 kWh) could, theoretically, power 7,050 homes for a year. Similarly, the storm of December 12, 2000 contained 2.3×10^7 kWh total potential energy, and the lagoon could supply a potential energy of 1.3×10^4 kWh, enough energy to power the equivalent of 22 homes for a month. A larger lagoon or multiple lagoons could capture more energy from the extreme surge events. The added benefit of the lagoon could be to reduce the flooding risk in coastal Lake Erie by routing the surge elevation.

As an example, the analysis of the lake-wide wave data for 2011 shows that the monthly mean wave power is greater in the central and eastern basins. The wave power was the highest in October and November when the monthly mean wave power reached at 10 kW/m. The wave power is reduced in winter mostly due to the presence of surface ice in the lake. The surface ice appears to significantly reduce wave height and power during winter months, resulting in a relatively low annual mean wave power. However, the monthly wave power was the lowest in late spring and during summer when the monthly mean wave power was estimated approximately 2.5 kW/m.

The analysis of the long-term wave characteristics and energy for three active buoys in Lake Erie show that the maximum hourly wave power increases from the western basin toward the eastern basin where the lake is deeper. For instance, buoy C45142 located further east demonstrates a maximum hourly wave height of more than 5 m and the maximum hourly wave power can reach up to 125 kW/m.

Since marine renewable energy technologies are still in their infancy, their costs are still significantly higher than conventional, and other renewable energy sources. The levelized cost of energy ($/MWh: the present value of all costs of a project divided by lifetime energy production) is commonly used to compare the cost of various energy technologies. While the average cost of some renewable energy sources such as onshore wind are about $80-120/MWh, and can be as low as conventional thermal power stations (*e.g.*, coal), new technologies such as offshore wind and marine renewables are still much more expensive (8e., $200-500/MWh;[46]). As the technology readiness level of an energy technology grows through investment in R&D, its cost and associated financial risks reduce. This trend can be clearly seen in the wind energy industry. Therefore, although the development of marine renewable energy projects at commercial scale may not be viable at present in Lake Erie, more research helps identify the potential for marine renewable development in this area in the form of demonstration projects. Also, future research can focus on site specific projects where additional cost of energy can be justified by coastal protection, as discussed. This study presented an assessment of the theoretical surge/seiche and wave energy in Lake Erie. Much research is still necessary to assess the technical and practical energy resources of the lake. In particular, suitable energy devices, environmental and socio-economic constraints should be investigated.

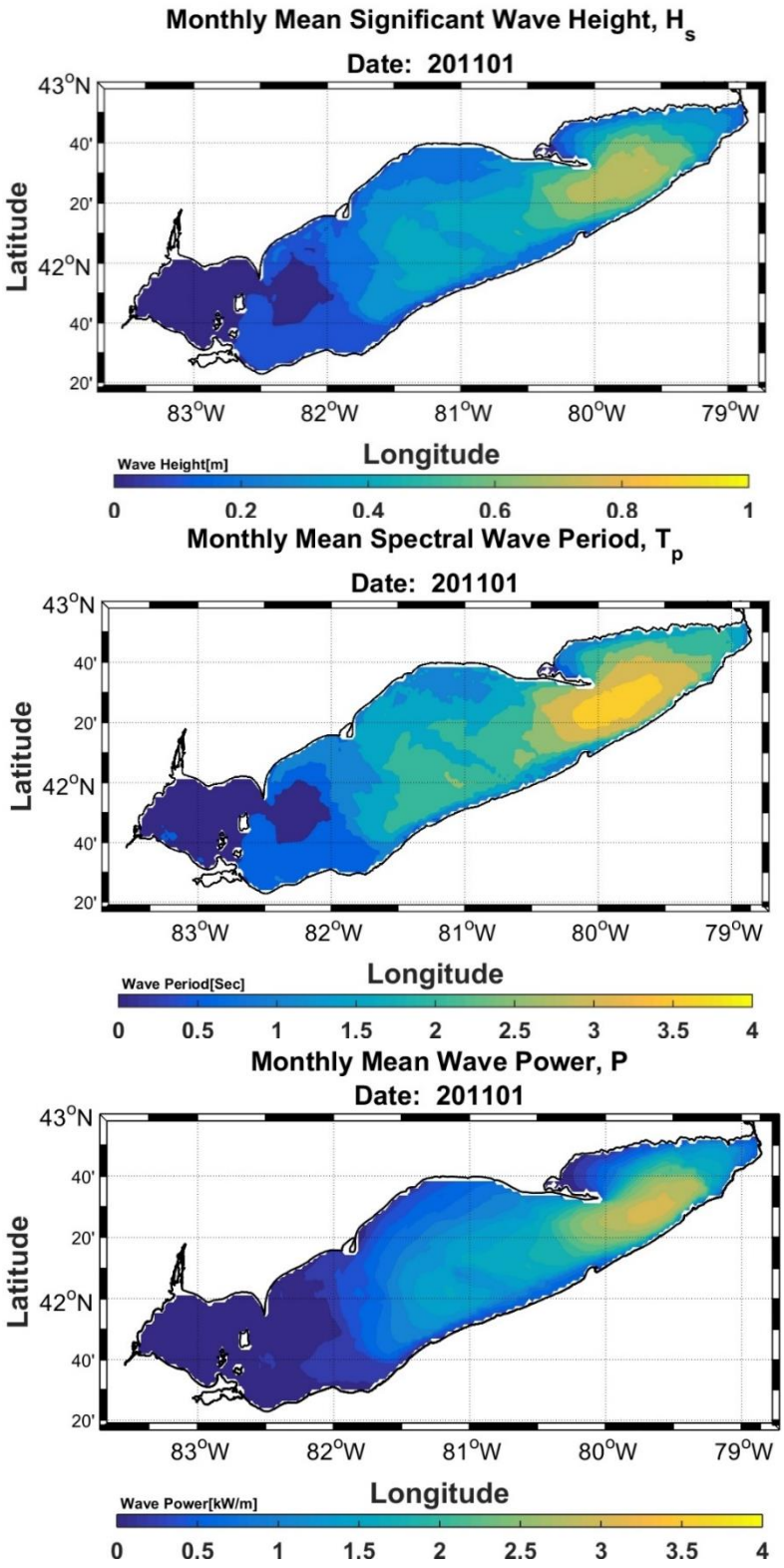

Figure 17. Spatial variations of monthly mean waves and wave power, January 2011

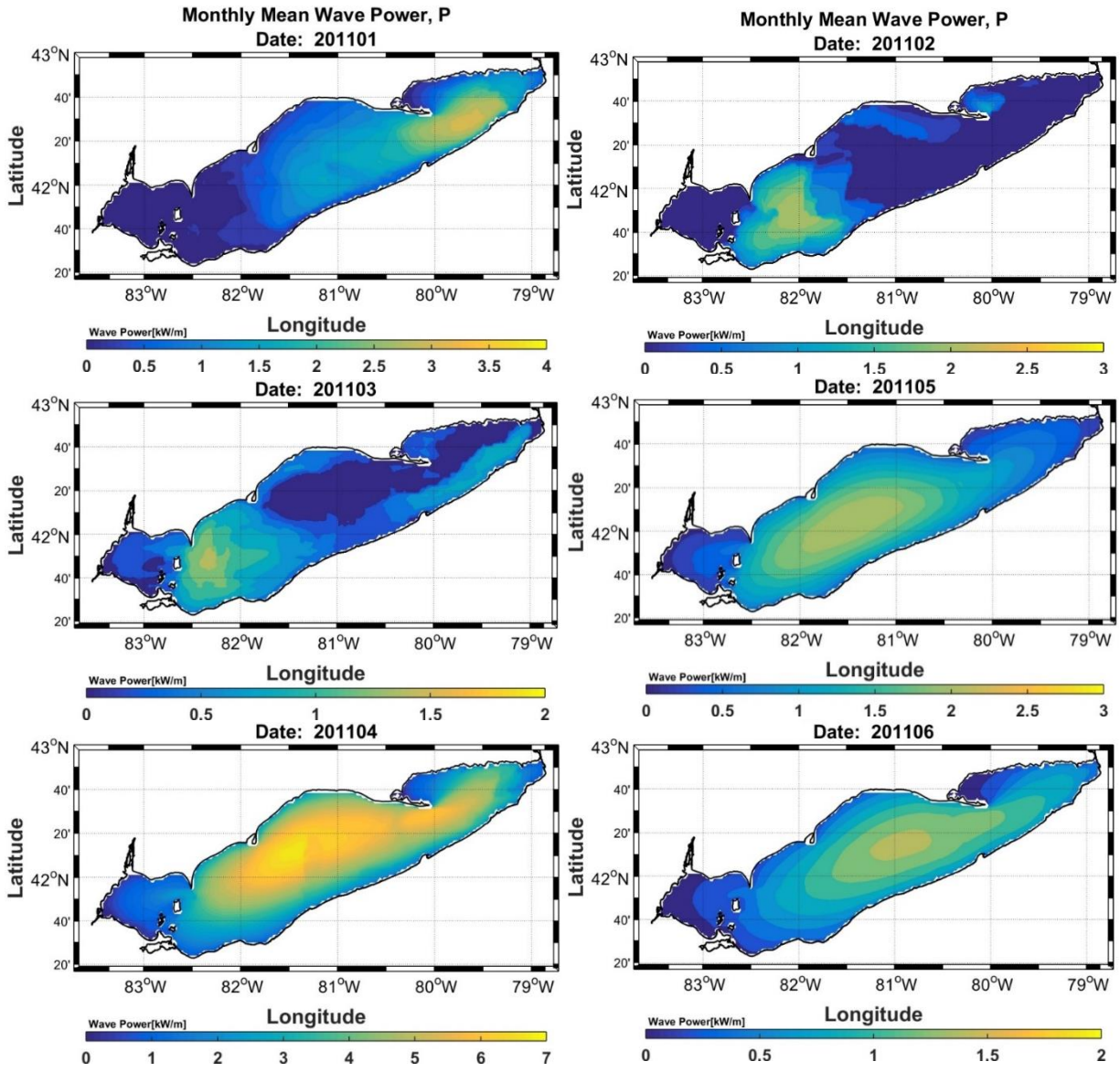

Figure 18. Spatial variations of monthly mean wave power, January-June 2011

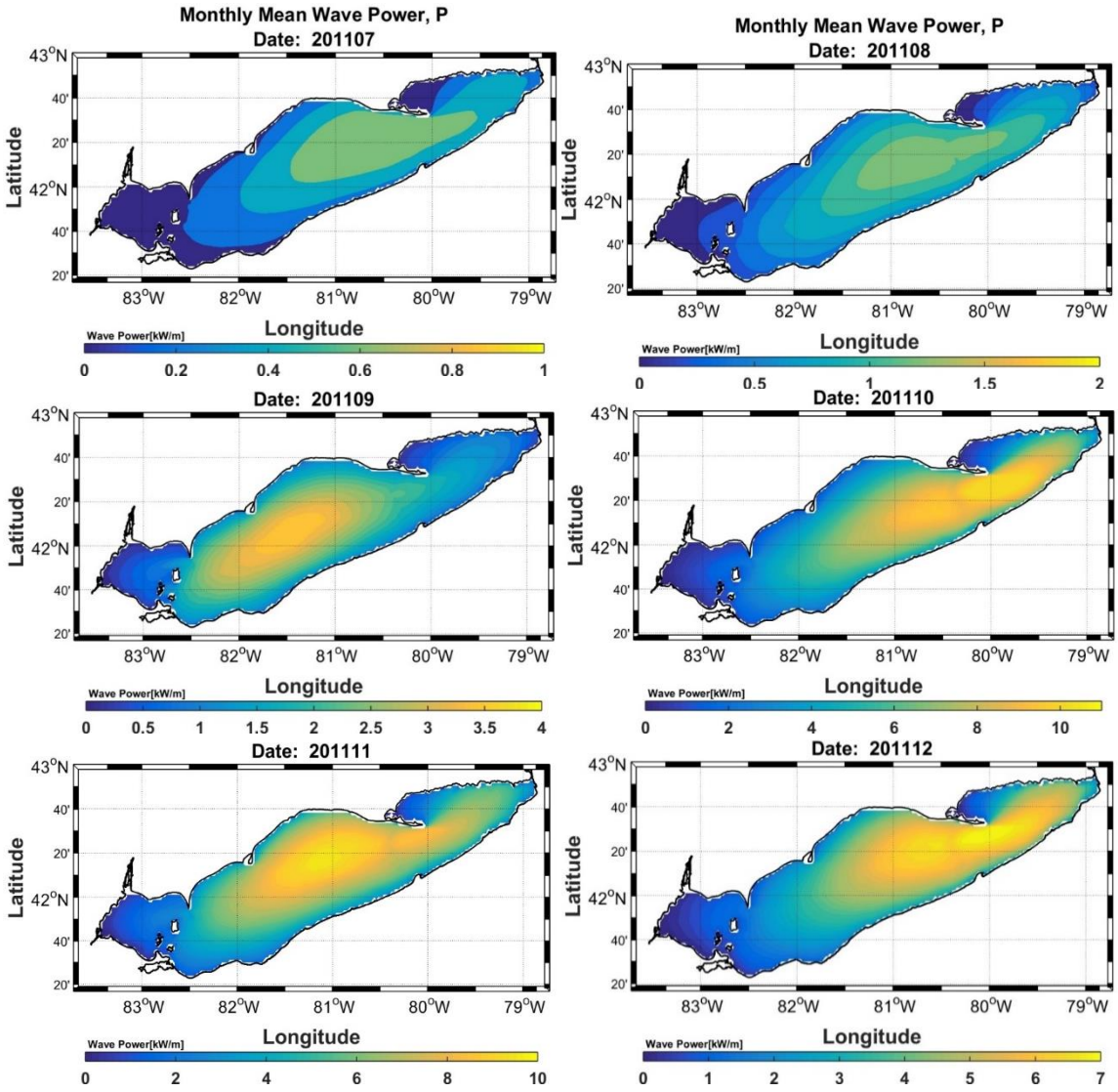

Figure 19. Spatial variations of monthly mean wave power, July-December 2011

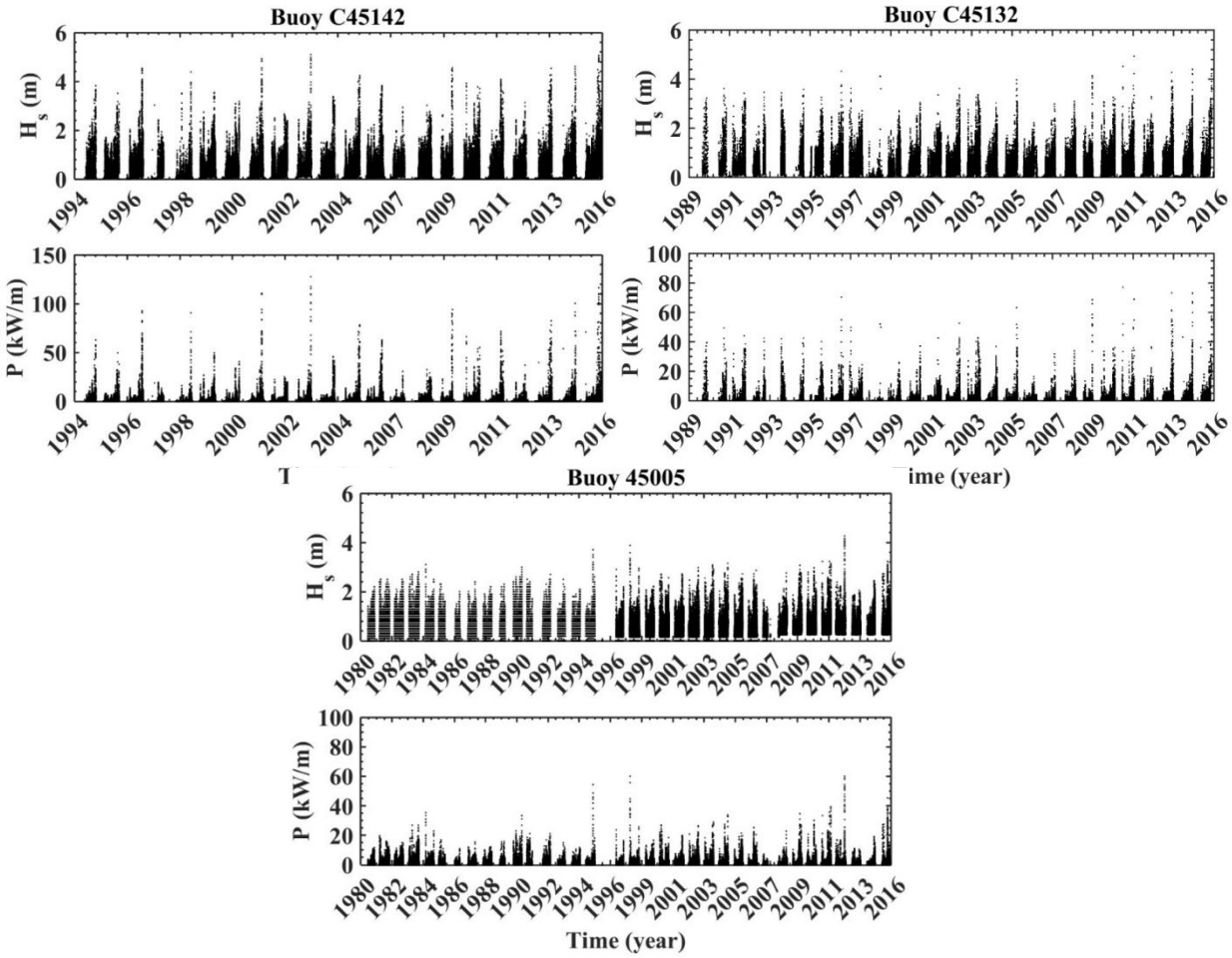

Figure 20. Long-term variations of wave height and power for Buoys C45142, C45132 and 45005

Acknowledgements
The authors would like to thank Dr. Robert E. Jensen of the U.S. Army Corps of Engineers, ERDC, for providing the WIS wave data.

REFERENCES

1. Electronic Power Research Institute (EPRI). (2011). *Mapping and Assessment of the United States Ocean Wave Energy Resource*. Palo Alto, CA: 1024637.
2. New York State Energy Research and Development Authority. (2014). Energy Efficiency and Renewable Energy Potential Study of New York State, Report Number 14-19.
3. Environmental Protection Agency Great Lakes Atlas, *accessed* at: http://epa.gov/greatlakes/atlas/index.html.
4. Lake Erie Energy Development Corporation (LEEDCo), accessed at: http://www.leedco.org/about
5. Gorsevski, P.V. and Mekonnen, A.D. (2015). "A web-based participatory GIS (PGIS) for offshore wind farm suitability within Lake Erie, Ohio", Renewable and Sustainable Energy Reviews 41 (2015): 162-177.
6. Waters, S. and Aggidis, G., 2016. A world first: Swansea Bay tidal lagoon in review. *Renewable and Sustainable Energy Reviews*, *56*, pp.916-921.
7. Andresen, J., Hilberg, S., and K. Kunkel. (2014). Historical Climate and Climate Trends in the Midwestern USA. In: Climate Change in the Midwest: A Synthesis Report for the National Climate Assessment, J.A. Winkler, J.A. Andresen, J.L. Hatfield, D. Bidwell, and D. Brown, eds., Island Press, 8-36.
8. Buffalo Architecture and History, The History of Buffalo: A Chronology; accessed at: http://www.buffaloah.com/h/1865.html
9. National Oceanic and Atmospheric Administration (NOAA), National Ocean Services; accessed at: http://oceanservice.noaa.gov/facts/seiche.html
10. Mortimer, C.H. (1987). "Fifty Years of Physical Investigations and Related Limnological Studies on Lake Erie, 1928–1977". J. Great Lakes Res. 13:4, 407-435.
11. Platzman, G. W., and Rao, D. B. (1964). "Spectra of Lake Erie Water Levels". J. Geophys. Res. 69, 2525-2533, 1964.
12. Platzman, G. W. (1966). "The Daily Variation of Water Level on Lake Erie". J. Geophys. Res. 71:2472-2483.
13. Kite, g. W. (1992). "Spectral Analysis of Selected Lake Erie Levels", J. Great Lakes Res. 18(1):207-217.
14. Henry, A. J. (1902). "Wind velocity and fluctuations of water level on Lake Erie", U. S. Weather Bureau, Bull. J.
15. Irish, S. M. and Platzman, G.W. (1962): "An Investigation of the Meteorological Conditions Associated with Extreme Wind Tides on Lake Erie", Mon. Wea. Rev., 90, 39–47.
16. Hamblin, P.F. (1987). "Meteorological Forcing and Water Level Fluctuations on Lake Erie, J. Great lakes Res. 13(4):436-453.
17. Farhadzadeh, A. (2017). "A study of Lake Erie seiche and low frequency water level fluctuations in the presence of surface ice", Ocean Engineering, 135 (2017) 117–136. http://dx.doi.org/10.1016/j.oceaneng.2017.02.027.
18. National Oceanic and Atmospheric Administration (NOAA), Great Lakes Environmental Research Laboratory, "Historical Ice Cover", accessed at: http://www.glerl.noaa.gov/data/ice/

19. National Oceanic and Atmospheric Administration (NOAA), Lake Erie and Lake Saint Clair Geomorphology, accessed at: https://www.ngdc.noaa.gov/mgg/greatlakes/lakeerie_cdrom/html/e_gmorph.htm

20. Assel, R.A. (2003). NOAA Atlas: An Electronic Atlas of Great Lakes Ice Cover, Winters: 1973-2002. NOAA, Great Lakes Environmental Research Laboratory, Ann Arbor, MI, 2 CD-ROM Set or DVD.

21. United States Army Corps of Engineers (USACE), Wave Information System (WIS); accessed at: http://wis.usace.army.mil/

22. National Oceanic and Atmospheric Administration (NOAA), National Data Buoy Center; accessed at: http://www.ndbc.noaa.gov/

23. Fisheries and Oceans Canada, Waves and other Moored Marine Buoy Observations, accessed at: http://www.meds-sdmm.dfo-mpo.gc.ca/isdm-gdsi/waves-vagues/index-eng.htm

24. Resio, D.T. (1981). "The Estimation of Wind-Wave Generation in a Discrete Spectral Model", The Journal of Physical Oceanography, 11:4, 510-525.

25. Hubertz, J.M. (1992). "User's Guide to the Wave Information Studies (WIS) Wave Model: Version 2.0", WIS Report 27, US Army Corps of Engineers, Waterways Experiment Station, Vicksburg, MS, 41 pp.

26. National Oceanic and Atmospheric Administration (NOAA), Tides and Currents, accessed at: http://tidesandcurrents.noaa.gov/stations.html?type=Water+Levels

27. Fisheries and Oceans Canada, Tides, Currents, and Water Levels, accessed at: http://www.tides.gc.ca/eng

28. Dietrich, J. C. et al. (2011). "Modeling Hurricane Waves and Storm Surge Using Integrally-Coupled, Scalable Computations", Coastal Engineering 58 (2011) 45–65.

29. Luettich, R.A. and J.J. Westerink. (1991). "A solution for the vertical variation of stress, rather than velocity, in a three-dimensional circulation model", International Journal for Numerical Methods in Fluids, 12:911-928.

30. Booij, N., Ris, R. C., and Holthuijsen, L. H., (1999). "A third-generation wave model for coastal regions: 1. Model description and validation", Journal of Geophysical Research: Oceans, 104(C4), 7649–7666. doi:10.1029/98jc02622.

31. National Oceanic and Atmospheric Administration (NOAA), National Center for Environmental Information, Great Lakes Bathymetry, accessed at: https://www.ngdc.noaa.gov/mgg/greatlakes/greatlakes.html

32. Saha, S., Moorthi, S., Pan, H-L. et al. (2010)."The NCEP climate forecast system reanalysis," Bulletin of the American Meteorological Society, vol. 91, pp. 1015–1057.

33. ADCIRC: A (Parallel) Advanced Circulation Model For Oceanic, Coastal And Estuarine Waters, accessed at: http://www.unc.edu/ims/adcirc/documentv47/ADCIRC_title_page.html

34. The National Land Cover Database (NLCD), The USGS Land Cover Institute (LCI), accessed at: http://landcover.usgs.gov/uslandcover.php

35. Garratt, J. R. (1977). Review of drag coefficients over oceans and continents. Monthly Weather Review, 105(7), 915–929. doi:10.1175/1520-0493(1977)105<0915:rodcoo>2.0.co;2.

36. Chapman, R. S.; Mark, D., and Cialone, A. (2005). Regional tide and storm-induced water level prediction study for the West Coast Alaska, U.S. Army Engineer Waterways Experiment Station, Vicksburg, MS, Draft Report to POA.

37. Birnbaum, G., and Lüpkes, C. (2002). A new parameterization of surface drag in the marginal sea ice zone. Tellus A(1), 54 , 107-123.

38. Gerbush, M. R.; Kristovich, D. A. R., and Laird, N. F. (2008). "Mesoscale boundary layer and heat flux variations over pack Ice–Covered Lake Erie". Journal of Applied Meteorology and Climatology, 47(2), 668–682. doi:10.1175/2007jamc1479.1.

39. Chapman, R. S.; Kim, S-C, and Mark, D. J., 2009. Storm-induced water level prediction study for the Western Coast of Alaska, U.S. Army Engineer Waterways Experiment Station, Vicksburg, MS, Draft Report to POA.

40. Farhadzadeh, A. and Gangai, J. (2017). "Numerical Modeling of Coastal Storms for Ice-Free and Ice-Covered Lake Erie", Journal of Coastal Research (in press), doi: 10.2112/JCOASTRES-D-16-00101.1.

41. Jensen, R.; Schneffer, N.; Smith, S.J.; Webb, D., and Ebersole, B. (2002). Engineering studies in support of Delong Mountain Terminal Project, US Army Engineer Research and Development Center, Vicksburg, MS, Report ERDC/CHL TR-02-26.

42. Lewis, M.J., Angeloudis, A., Robins, P.E., Evans, P.S. and Neill, S.P., 2017. "Influence of storm surge on tidal range energy". Energy (in press). http://dx.doi.org/10.1016/j.energy.2017.01.068.

43. Clark, R. H. Elements of tidal-electric engineering. Vol. 33. John Wiley & Sons, 2007.

44. Hashemi, M. R., Grilli, S. T., and Neill, S. P., "A simplified method to estimate tidal current effects on the ocean wave power resource", Renewable Energy 96 (2016): 257-269.

45. Gross, J., Heckert, A. Lechner, J., and Simiu, E., (1994), "Novel Extreme Value Procedures: Application to Extreme Wind Data," in Extreme Value Theory and Applications, Vol. 1 (J.Galambos, J. Lechner andE. Simiu, eds.), Kluwer Academic Publishers, Dordrecht and Boston, 1994.

46. Chu, Steven, and Arun Majumdar. "Opportunities and challenges for a sustainable energy future." *nature* 488.7411 (2012): 294-303.